

RESEARCH LETTER

Loss of PTEN Signaling in Foxl1⁺ Mesenchymal Telocytes Initiates Spontaneous Colonic Neoplasia in Mice



Studies of colorectal cancer (CRC) traditionally focused on the role of epithelial genetic mutations and signaling pathway dysregulation with an underappreciation of faulty signaling impact from the stromal microenvironment in this context.¹ The colonic stroma consists of professional and nonprofessional cells with fibroblasts, myofibroblasts, and telocytes found in close contact with the epithelia.^{2,3} These latter cells are responsible for the contribution of the microenvironment surrounding the epithelium. The central role played by nonmyofibroblastic Foxl1⁺ telocytes as the source of indispensable intestinal stem cell niche factors was shown recently.^{3,4} Although mutation of *PTEN* in epithelium of various organs leads to cancer development, we and others showed that specific intestinal epithelial cell ablation of *Pten* is insufficient to initiate neoplasia.^{5,6} Such observations on epithelial phosphatase and tensin homolog deleted on chromosome 10 (*PTEN*) signaling suggest a greater role for extra-epithelial signaling in gut tumor development.

Here, using the *Foxl1*Cre recombinase, we generated a mouse model featuring a specific deletion of *Pten* in gut telocytes (*Pten*^{ΔFoxl1+}) (Supplementary Figure 1), allowing dissection of the specific contribution of PTEN signaling in colonic telocytes. As previously shown with abrogation of *Bmpr1a*^{ΔFoxl1+},^{7,8} and herein with *Pten*, the deregulation of important cell signaling in gut telocytes strongly impacted colon epithelial homeostasis (Figure 1). By 75 days, *Pten*^{ΔFoxl1+} colon spontaneously developed an average of 28 polyps as opposed to none in controls. Although normal colonic mucosal architecture was observed in both control and *Pten*^{ΔFoxl1+} mice, mutants showed

regions developing into lesions characterized by gut-associated lymphoid tissues, epithelial hyperplasia developing into benign lymphoid aggregates, and hamartomatous polyps composed of a mixture of epithelial and mesenchymal cells. These non-neoplastic lesions did not progress to carcinoma with age and were histologically similar to human hamartomatous polyps described in Cowden's disease. Thus, telocyte PTEN signaling is a key singular protective pathway against colonic polyposis initiation.

Studies showed that telocytes play a crucial role in secreting epithelial-interacting factors.^{3,4} Disruption of PTEN signaling in telocytes altered the subepithelial milieu (Supplementary Figure 2). Proliferating cell nuclear antigen immunostaining showed increases in the number of proliferating cells in the epithelium (3.18-fold) and surrounding mesenchyme (1.45-fold) in mutants when compared with controls. Co-immunostaining of vimentin and α -smooth muscle actin showed a remodeling of nonprofessional cell populations in mutants compared with controls. Nonprofessional cells are strongly bioactive through secretion of soluble factors impacting the extracellular milieu supporting epithelial cells. To investigate for precocious altering events, mucosa of 30-day-old control and *Pten*^{ΔFoxl1+} mice were analyzed for deregulated production of secreted factors. Altered expression of growth factors, extracellular matrix remodeling factors, cytokines, and chemokines was observed in *Pten*^{ΔFoxl1+} mice (Supplementary Tables 1 and 2). By deleting PTEN signaling in telocytes, we show how these cells play a key role in regulating the secretion of epithelial, stromal, and immune cell interacting soluble factors, promoting a potent tumor microenvironment without pre-existing epithelial hyperplasia.

Because *Pten*^{ΔFoxl1+} mice only develop benign polyps without cancerous progression, we hypothesized that the absence of *Pten* in telocytes in concert with a mutated epithelium could enable the

evolution of the cancer cascade. The generation of compound mutant mice with *Pten*^{ΔFoxl1+} and an ubiquitous *Apc*^{Min/+} mutation uncovered key synergistic cross-talk between defective subepithelial mesenchyme and a primed oncogenic epithelium, impacting epithelial tumor multiplicity (Figure 2). Our results show that at 75 days (compound mice died at approximately 85 days), this double mutation (*Pten*^{ΔFoxl1+}; *Apc*^{Min/+}) leads to accelerated polyposis initiation compared with *Apc*^{Min/+} animals (average, 18 and 3 adenomas, respectively), although no polyps were found in controls. This particular genetic combination is not sufficient to enable malignant transformation of a pre-neoplastic epithelium at 75 days of age. This could be explained by the limited life expectancy of the compound mice. This short latency is indubitably detrimental to the acquisition of key mutations allowing tumor progression. Second, the use of a different genetic epithelial mutation in combination with our dysfunctional mesenchyme should be explored. The serrated mouse models of CRC feature tumors that progress into adenocarcinomas with metastasis potential.^{9,10} Serrated CRC involves initial mutations such as *KRAS* or *BRAF*, but not *APC*. Because the loss of PTEN signaling in telocytes lead to an epithelial hyperplasia within 85 days, its association with epithelial mutations of the serrated route potentially could lead to the formation of more invasive lesions.

The present results indicate that loss of *Pten* in telocytes is sufficient to trigger the development of spontaneous colonic polyposis. Our findings further support that telocytes abrogated for PTEN signaling feature an altered stroma cell ratio and secretory profile leading to the establishment of a toxic microenvironment impacting colonic epithelial homeostasis. The current observations suggest that synergy between *Pten*-deficient telocytes and an oncogenically primed epithelium toward cancer progression may require a mutation from pathways such as the serrated route, as opposed

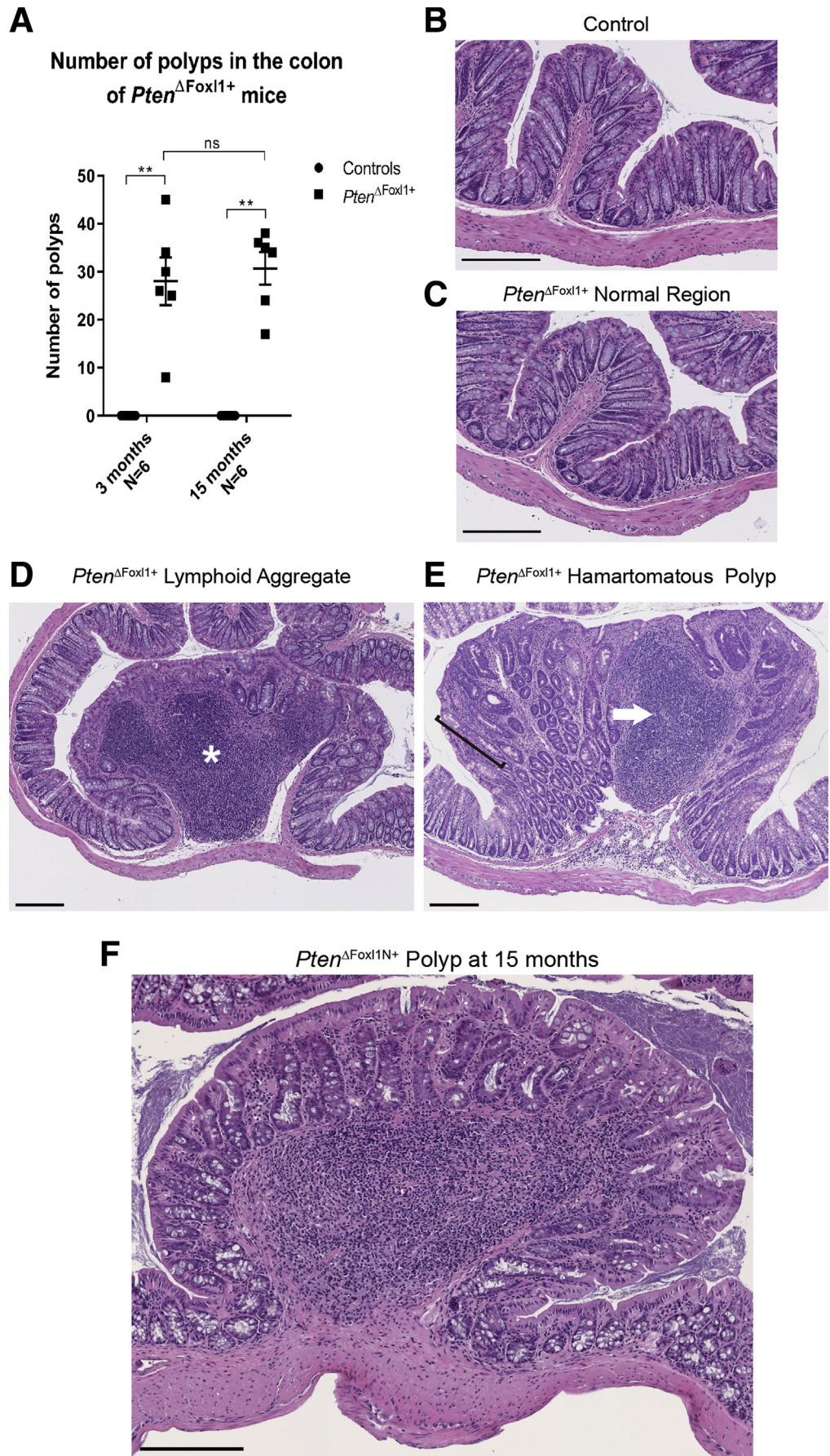


Figure 1. *Pten*^{ΔFoxl1+} mice develop spontaneous polyps in their colon by 75 days. (A) Polyps were counted from 3- and 15-month control and *Pten*^{ΔFoxl1+} colons. H&E staining of (B) control and (C) *Pten*^{ΔFoxl1+} normal colonic mucosa. (D) Lymphoid aggregates in *Pten*^{ΔFoxl1+} colon featured large gut-associated lymphoid tissues (white asterisk) and epithelial hyperplasia. (E) Hamartomatous polyps showed a mixture of epithelial and mesenchymal cells, longer crypts (black bracket), and immune cell infiltrates (white arrow). (F) Polyps in 15-month-old mutants did not progress into carcinoma. Data are expressed as means ± SEM. Mann-Whitney *U* test: ***P* ≤ .01. Scale bars: 200 μm.

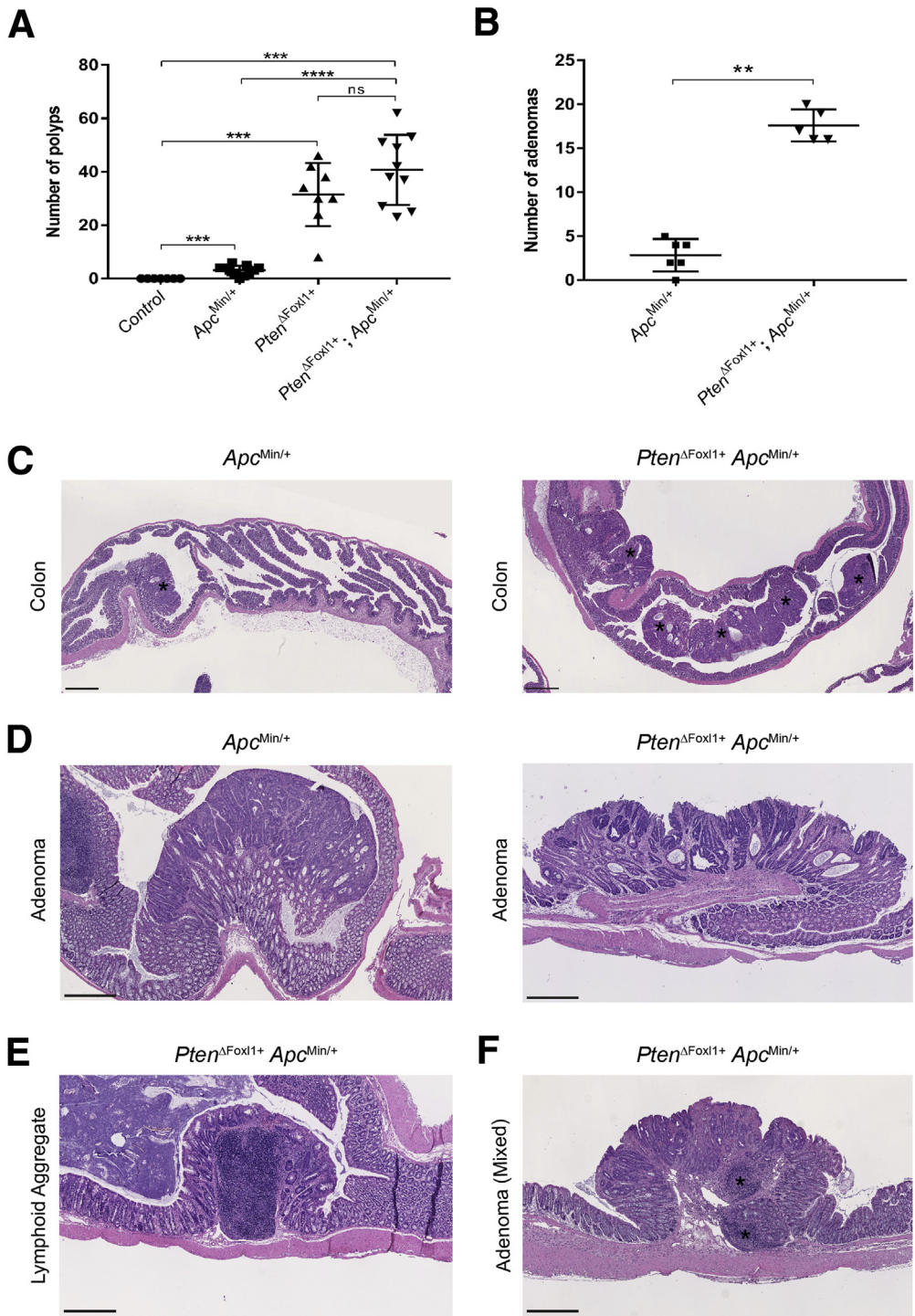


Figure 2. *Pten*-deficient telocytes and *Apc^{Min/+}* mutation increases adenoma multiplicity but not epithelial transformation in mice. Total (A) colonic polyps and (B) adenomas were counted from 75-day-old *Apc^{Min/+}*, *Pten^{ΔFoxl1+}*, and *Pten^{ΔFoxl1+}; Apc^{Min/+}* mice. (C) Histologic assessment showed an increase of adenoma multiplicity in *Pten^{ΔFoxl1+}; Apc^{Min/+}* when compared with *Apc^{Min/+}* colons (N = 6 and 5, respectively). Asterisks indicate adenomatous polyps. (D) All *Apc^{Min/+}* polyps were assessed histologically as adenomas. (E) Adenomas, (F) lymphoid aggregates, and (F) a mixed adenoma were found in *Pten^{ΔFoxl1+}; Apc^{Min/+}* colons. Data are expressed as means ± SEM. Mann-Whitney U test: ***P* ≤ .01, ****P* ≤ .001, and *****P* ≤ .0001. Scale bars: (A) 1 mm, (D–F) 500 μm.

to the traditional pathway involving APC mutation.

MARIE-JOSÉE LANGLOIS,¹
 RAPHAËLLE SERVANT,¹ VILCY REYES
 NICOLÁS,¹ CHRISTINE JONES,¹ SÉBAS-
 TIEN A.B. ROY,¹ MARILÈNE PAQUET,²
 JULIE C. CARRIER,³ NATHALIE RIVARD,¹
 FRANCOIS BOUDREAU,¹
 NATHALIE PERREAULT,¹

¹Département d'Anatomie et Biologie Cellulaire, ³Département de Médecine, Faculté de Médecine et des Sciences de la Santé, Université de Sherbrooke, Sherbrooke, Quebec, Canada; ²Département de Pathologie et de Microbiologie, Faculté de Médecine Vétérinaire, Université de Montréal, St-Hyacinthe, Quebec, Canada


Corresponding author: e-mail: Nathalie.Perreault@USherbrooke.ca.

References

1. Taddei ML, et al. *Cancer Lett* 2013; 341:80–96.
2. McLin VA, et al. *Gastroenterology* 2009;136:2074–2091.

3. Shoshkes-Carmel M, et al. *Nature* 2018;557:242–246.
4. Aoki R, et al. *Cell Mol Gastroenterol Hepatol* 2016;2:175–188.
5. Langlois MJ, et al. *FASEB J* 2009;23:1835–1844.
6. Marsh V, et al. *Nat Genet* 2008;40:1436–1444.
7. Allaire JM, et al. *Int J Cancer* 2016;138:2700–2712.
8. Roy SA, et al. *Sci Rep* 2016;6:32759.
9. Davies EJ, et al. *J Pathol* 2014;233:27–38.
10. Jackstadt R, et al. *J Pathol* 2016;238:141–151.

Abbreviations used in this letter: CRC, colorectal cancer; PTEN, phosphatase and tensin homolog deleted on chromosome 10

 **Most current article**

© 2019 The Authors. Published by Elsevier Inc. on behalf of the AGA Institute. This is an open access article under the CC BY-NC-ND license (<http://creativecommons.org/licenses/by-nc-nd/4.0/>).
2352-345X
<https://doi.org/10.1016/j.jcmgh.2019.05.007>

Received April 17, 2019. Accepted May 21, 2019.

Author contributions

Marie-Josée Langlois, Nathalie Rivard, Francois Boudreau, Julie C. Carrier, and Nathalie Perreault conceived and designed the experiments; Marie-Josée Langlois contributed to results shown in [Figures 1](#) and [2](#), [Supplementary Figures 1](#) and [2](#), and [Table 1](#); Raphaëlle Servant contributed to

results shown in [Supplementary Figures 1](#) and [2](#); Vilcy Reyes-Nicolas and Christine Jones contributed to results shown in [Supplementary Table 2](#); Sébastien A. B. Roy contributed to results shown in [Figures 1](#) and [2](#); Marie-Josée Langlois, Vilcy Reyes-Nicolas, Christine Jones, Marilène Paquet, Nathalie Rivard, Julie C. Carrier, Francois Boudreau, and Nathalie Perreault analyzed the data; Nathalie Rivard, Francois Boudreau, and Nathalie Perreault contributed to reagents/materials/analysis tools; Raphaëlle Servant contributed to figure preparation; and Nathalie Perreault prepared and wrote the manuscript. All authors reviewed the manuscript.

Conflicts of interest

The authors disclose no conflicts.

Funding

This research was supported by the Cancer Research Society (N.P., F.B., J.C.C., and N.R.), and the Canadian Institutes of Health Research MOP-136917 (N.P.).

Supplementary Materials and Methods

Animals

C57BL/6-*Apc*^{Min/+} (002020) and BALB/*c-Pten*^{fx/fx} (004597) mice were purchased from The Jackson Laboratory (Bar Harbor, ME). The C57BL/6J *Foxl1Cre* transgenic line was provided by Dr K. H. Kaestner.¹ BALB/*c-Pten*^{fx/fx} mice were backcrossed with C57BL/6J mice for more than 18 generations. All mutations were genotyped according to a previously published protocol¹ or as directed by The Jackson Laboratory. All experiments were approved by the Animal Research Committee of the Faculty of Medicine and Health Sciences of the Université de Sherbrooke (Animal welfare committee approval number FMSS-308-17). The study followed the standards and policies of the Canadian Council on Animal Care in sciences.

Polyp Counts

Methylene blue-stained polyps were visualized under a stereomicroscope. Polyp sizes were measured with a digital caliper (Fisher Scientific, Waltham, MA) and polyp numbers were counted from the duodenum to the rectum as previously described.^{2,3}

Histologic Staining, Immunohistochemistry, and Immunofluorescence

Tissues were fixed, paraffin-embedded, sectioned, and stained as described previously.^{2,4-9} Immunohistochemistry staining of proliferating cell nuclear antigen (18197; Abcam, Cambridge, MA), anti- α -smooth muscle actin (A2547; Sigma-Aldrich, Oakville, ON, Canada), and antivimentin (5741; Cell Signaling Technology, Danvers, MA) were performed as previously

described.^{2,4-10} Immunofluorescence against PTEN (9559; Cell Signaling) and α -smooth muscle actin (A2547; Sigma) was performed on optimal cutting temperature-embedded tissues as previously described.⁴ Alexa Fluor-conjugated antibodies for all immunofluorescence studies were obtained from Invitrogen (Carlsbad, CA). Immunofluorescence images were acquired with a Leica (Leica Microsystems Inc, Concord, ON, Canada) DLMB2 microscope equipped with a DFC300FX camera and Leica FireCAM 3.4.1 software. Otherwise, slides were visualized with a NanoZoomer slide scanner and NDP.view2 software (Hamamatsu Corporation, Bridgewater, NJ).

Cytokine and Chemokine Assays

Cytokine and chemokine production was determined with antibody arrays from RayBiotech (Peachtree Corners, GA) according to the manufacturer's protocols. The Mouse Cytokine Array G1000 was used on total protein extracts from the colon of 30-day-old mutant and control mice. The arrays were scanned with the Cy3 channel using a ScanArray Express dual-color confocal laser scanner and ScanArray Express software (PerkinElmer, Waltham, MA).

RNA Extraction and Gene Expression Analysis

Total RNA was isolated and processed using the Totally RNA extraction kit (Ambion, Carlsbad, CA). Reverse-transcription polymerase chain reaction and quantitative real-time polymerase chain reaction were performed as described previously.^{2,4-9} For every quantitative polymerase chain reaction run, a no-template control was

performed for each primer pair, each of which was consistently negative. Primer sequences are available upon request.

Data Analysis

All epithelial cell counts were performed on well-oriented crypts. To determine the ratio of proliferative mesenchymal cells shown in [supplementary Figure 2](#), the number of proliferating cell nuclear antigen-positive cells relative to the total number of mesenchymal cells in a defined area was counted. Statistical tests used are described in figure legends. Data are expressed as means \pm SEM. Graphs and statistics were generated with GraphPad Prism (GraphPad Software Inc, San Diego, CA). All authors had access to the study and reviewed and approved the final manuscript.

References

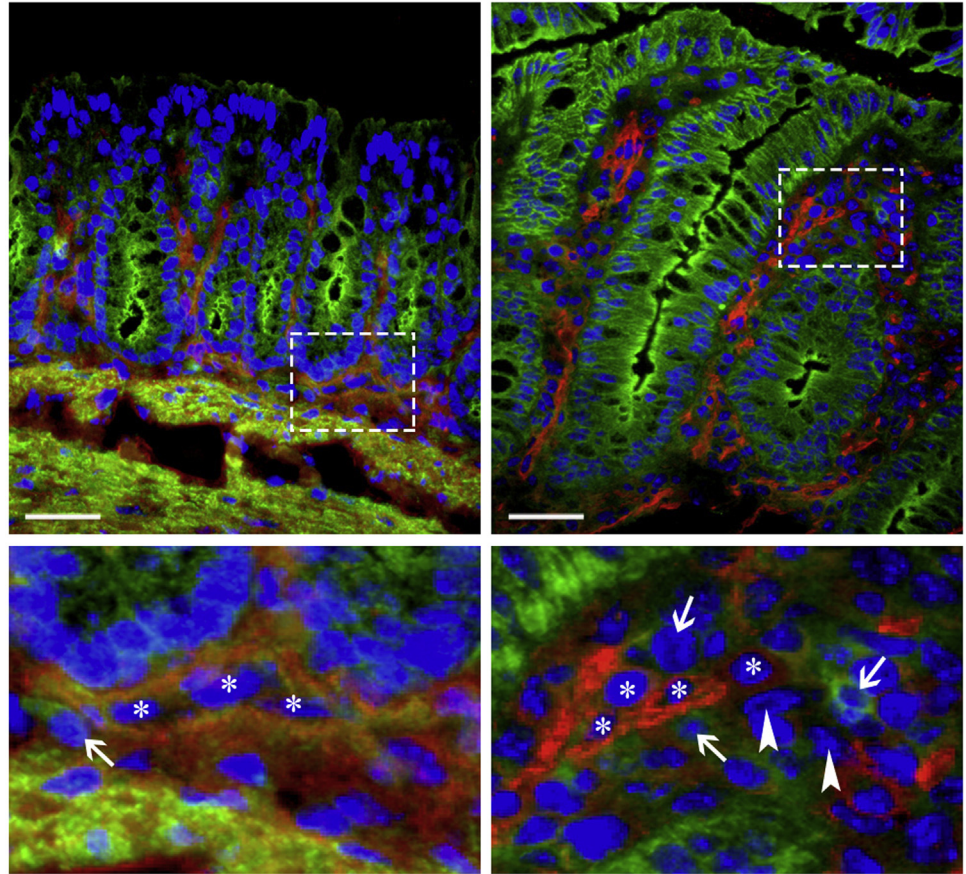
1. Sackett SD, et al. *Genesis* 2007; 45:518–522.
2. Langlois MJ, et al. *FASEB J* 2009; 23:1835–1844.
3. Perreault N, et al. *Genes Dev* 2005;19:311–315.
4. Allaire JM, et al. *Am J Physiol Gastrointest Liver Physiol* 2011; 300:G586–G597.
5. Allaire JM, et al. *Int J Cancer* 2016;138:2700–2712.
6. Auclair BA, et al. *Gastroenterology* 2007;133:887–896.
7. Gagne-Sansfacon J, et al. *PLoS One* 2014;9:e98751.
8. Maloum F, et al. *Am J Physiol Gastrointest Liver Physiol* 2011; 300:G1065–G1079.
9. Roy SA, et al. *Sci Rep* 2016; 6:32759.
10. Coulombe G, et al. *Mol Cell Biol* 2013;33:2275–2284.

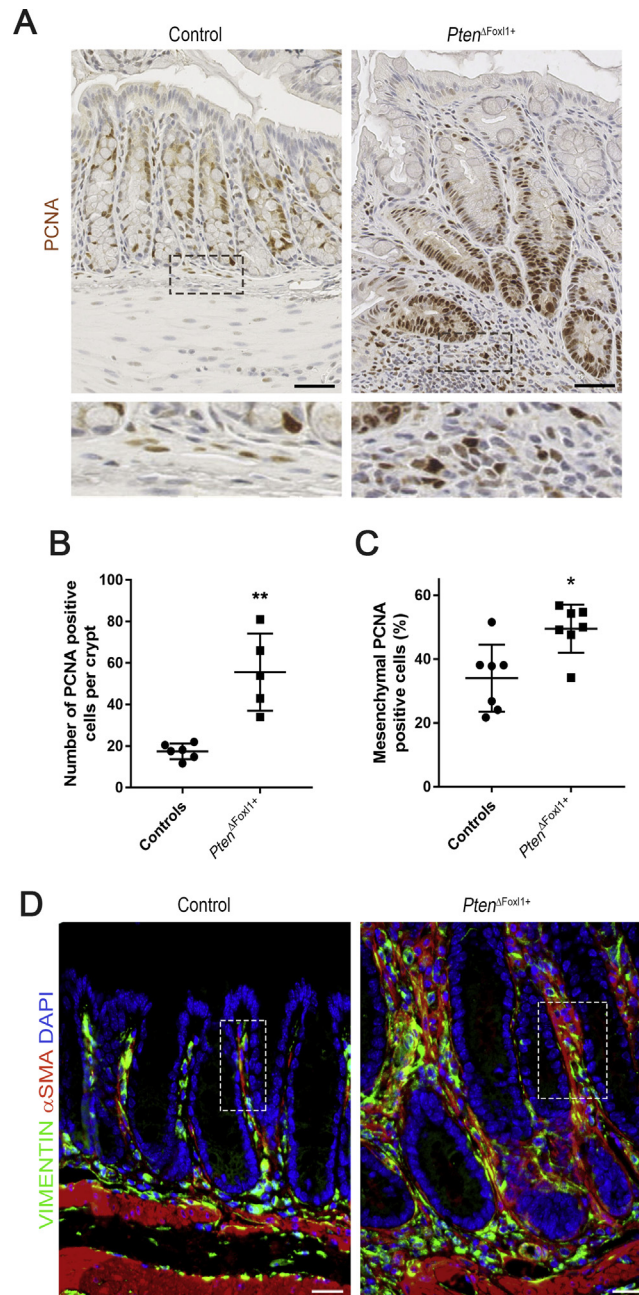
Control

Pten^{ΔFoxl1+}

Supplementary Figure 1. Validation of the loss of PTEN in colonic telocytes of *Pten*^{ΔFoxl1+} mice. PTEN immunostaining (signal in green) is observed in the epithelium of both control and *Pten*^{ΔFoxl1+} mice. Co-staining of PTEN and α-smooth muscle actin (αSMA) (signal in red) showed that immunoreactivity to PTEN was specifically lost in some αSMA⁻ mesenchymal cells (*white arrowheads*) as opposed to αSMA⁺ mesenchymal cells (*white asterisks*) and other αSMA⁻ mesenchymal cells (*white arrows*) corresponding to fibroblasts, which retain PTEN expression in *Pten*^{ΔFoxl1+} mice. Control mice showed PTEN immunoreactivity in αSMA⁻ (*white arrow*) and αSMA⁺ (*white asterisks*) mesenchymal cells. Scale bars: 25 μm. DAPI, 4',6-diamidino-2-phenylindole.

PTEN αSMA DAPI





Supplementary Figure 2. Increased mucosal proliferation and mesenchymal cellular remodeling in $Pten^{\Delta Foxl1+}$ mice.

(A) Proliferation was analyzed by immunohistochemistry using a proliferating cell nuclear antigen (PCNA) antibody in 75-day-old control and $Pten^{\Delta Foxl1+}$ mice. Proliferative cells (brown signal) were found in a very limited number of pericryptal mesenchymal cells in control mice. Cell counts of PCNA-stained cells showed a significant increase in the number of proliferating cells in the (B) epithelium of hyperplastic crypts (3.18-fold) ($N = 5$) and in the (C) mesenchyme (1.45-fold) of $Pten^{\Delta Foxl1+}$ mice ($N = 7$) compared with controls ($N = 6$ and $N = 7$, respectively). (D) Co-immunostaining against α -smooth muscle actin (α SMA) (red staining, muscle cells, and myofibroblasts) and vimentin (green staining, fibroblasts, Foxl1⁺ cells, and myofibroblasts) was performed on colonic sections of control and $Pten^{\Delta Foxl1+}$ mice. Myofibroblasts (yellow), fibroblasts, and Foxl1⁺ cells (green) and muscle cells (red) were present in the mesenchyme of both control and mutant mice, with a robust increase in all cell types in polyp pericryptal mesenchyme of $Pten^{\Delta Foxl1+}$ mice. For example, in the delimited areas, epithelial cells represent 71%, fibroblasts and Foxl1⁺ cells represent 14%, myofibroblasts represent 5%, and muscle cells represent 10% of all cells in the control mouse compared with 50% of epithelial cells, 18% of fibroblasts and Foxl1⁺ cells, 20% of myofibroblasts, and 12% of muscle cells in the mutant mouse. Error bars represent SEM (Mann–Whitney U test: * $P < .05$; ** $P < .01$). Five to 10 crypts per mouse were counted and each dot represents the average for 1 mouse. Scale bars: (A) 50 μ m and (D) 25 μ m. DAPI, 4',6-diamidino-2-phenylindole.

Supplementary Table 1. Modulated Cytokines/Chemokines in Colons of 30-Day-Old *Pten*^{ΔFoxl1+} Mice

Factors	Fold change	P value
Growth factors and growth factor regulators		
Insulin like growth factor binding protein 5	3.22	.001
Insulin like growth factor binding protein 6	-5.26	.005
Osteoprotegerin	1.74	.034
Stromal cell-derived factor 1/chemokine (C-X-C motif) ligand 12	6.14	.012
Soluble tumor necrosis factor receptor II	1.47	.026
TROY	1.86	.004
Thymic stromal lymphopietin	2.09	.001
Vascular endothelial growth factor A	1.98	.042
Vascular endothelial growth factor receptor 2	3.87	.011
Extracellular matrix remodeling factors		
Matrix metalloproteinase 3	11.71	.003
Pro-matrix metalloproteinase 9	14.14	1.45E-05
Tissue inhibitors of metalloproteinases-1	4.42	.014
Tissue inhibitors of metalloproteinases-2	-2.59	.062
Inflammatory cytokines and chemokines		
BLC	28.39	.050
CD30 ligand	8.63	.005
CD40	2.06	.004
EOTAXIN/chemokine (C-C motif) ligand 11	2.93	.004
Glucocorticoid-induced TNFR family related gene	2.15	2.0E-04
Granulocyte-macrophage colony stimulating factor	4.65	.001
Interleukin 4	17.13	.049
Interleukin 6	17.19	.050
Interleukin 9	6.43	.002
Interleukin 12	1.74	.012
Interleukin 13	6.67	.129
Interleukin 15	1.82	.001
Interferon-inducible T cell alpha chemoattractant/chemokine (C-X-C motif) ligand 11	-2.51	.039
L-selectin	5.92	.008
Lymphotactin	19.80	.039
Monocyte chemoattractant protein 1/ chemokine (C-C motif) ligand 2	22.77	.001
Monocyte Chemoattractant Protein 5/ Chemokine (C-C motif) Ligand 12	7.53	.00022
Macrophage-derived chemokine/ chemokine (C-C motif) ligand 22	11.65	.005
Monokine induced by Gamma/Chemokine (C-X-C motif) ligand 9	6.30	.026
Regulated on activation, normal T cell expressed and secreted	2.42	.004

NOTE. Fold change represents the ratio of mean value (mutant/control) of cytokine/chemokine expression analyzed using the RayBiotech Mouse Cytokine Antibody Array G series 1000 on total colonic protein extracts from 30-day-old mice (N = 4). Negative values indicate a reduction in *Pten*^{ΔFoxl1+} mice compared with controls. Statistical probability was determined using the Student *t* test.

Supplementary Table 2. Gene Expression Levels of Secreted Factors in Colons of 30- to 45-Day-Old *Pten*^{ΔFoxl1+} Mice

Factors	Fold change	P value
Growth factors and growth factors regulators		
Insulin like growth factor binding protein 5	20.70	.008
Insulin like growth factor binding protein 6	-0.74	.206
Stromal cell-derived factor 1/ chemokine (C-X-C motif) ligand 12	1.05	.841
TROY	1.50	.691
Vascular endothelial growth factor A	1.05	.042
Extracellular matrix remodeling factors		
Pro-matrix metalloproteinase 9	41.70	.008
Tissue inhibitors of metalloproteinases-1	7.00	.008
Tissue inhibitors of metalloproteinases-2	1.72	.056
Inflammatory cytokines and chemokines		
Interleukin 13	40.05	.036
Interleukin 15	1.18	.548
Monocyte chemoattractant protein 5/chemokine (C-C motif) ligand 12	6.03	.016
Monokine induced by Gamma/ chemokine (C-X-C motif) ligand 9	23.05	.079
EOTAXIN/chemokine (C-C motif) ligand 11	2.47	.064

NOTE. Fold change represents the ratio of mean value (mutant/control) of total colonic RNA extracts from 30- to 45-day-old mice (N = 5). Negative values indicate a reduction in *Pten*^{ΔFoxl1+} mice compared with controls. Statistical probability was determined using the Student *t* test.